Control of optical bandgap energy and optical absorption coefficient by geometric parameters in sub-10 nm silicon-nanodisc array structure

2012 Nanotechnology 23 065302

(http://iopscience.iop.org/0957-4484/23/6/065302)

Nanotechnology **23** (2012) 065302 (6pp) doi:10.1088/0957-4484/23/6/065302

Control of optical bandgap energy and optical absorption coefficient by geometric parameters in sub-10 nm silicon-nanodisc array structure

Mohd Fairuz Budiman[1,2], Weiguo Hu[1,2], Makoto Igarashi[1,2], Rikako Tsukamoto[1,2], Taiga Isoda[2,3], Kohei M Itoh[2,3], Ichiro Yamashita[2,4], Akihiro Murayama[2,5], Yoshitaka Okada[2,6] and Seiji Samukawa[1,2]

[1] Institute of Fluid Science, Tohoku University, 2-1-1 Katahira, Aoba-ku, Sendai, Miyagi 980-8577, Japan
[2] Japan Science and Technology Agency (JST), CREST, 5 Sanbancho, Chiyoda, Tokyo 102-0075, Japan
[3] Department of Applied Physics and Physico-Informatics, Keio University, 3-14-1 Hiyoshi, Kouhoku-ku, Yokohama 223-8522, Japan
[4] Advanced Technology Research Laboratories, Panasonic Co., Ltd., 3-4 Hikari-dai, Seika, Kyoto 619-0237, Japan
[5] Graduate School of Information Science and Technology, Hokkaido University, N14 W9, Kita-ku, Sapporo 060-0814, Japan
[6] Research Center for Advanced Science and Technology, The University of Tokyo, 4-6-1 Komaba, Megaro-ku, Tokyo 153-8904, Japan

E-mail: samukawa@ifs.tohoku.ac.jp

Received 24 October 2011, in final form 18 December 2011
Published 17 January 2012
Online at stacks.iop.org/Nano/23/065302

Abstract
A sub-10 nm, high-density, periodic silicon-nanodisc (Si-ND) array has been fabricated using a new top-down process, which involves a 2D array bio-template etching mask made of *Listeria*-Dps with a 4.5 nm diameter iron oxide core and damage-free neutral-beam etching (Si-ND diameter: 6.4 nm). An Si-ND array with an SiO_2 matrix demonstrated more controllable optical bandgap energy due to the fine tunability of the Si-ND thickness and diameter. Unlike the case of shrinking Si-ND thickness, the case of shrinking Si-ND diameter simultaneously increased the optical absorption coefficient and the optical bandgap energy. The optical absorption coefficient became higher due to the decrease in the center-to-center distance of NDs to enhance wavefunction coupling. This means that our 6 nm diameter Si-ND structure can satisfy the strict requirements of optical bandgap energy control and high absorption coefficient for achieving realistic Si quantum dot solar cells.

(Some figures may appear in colour only in the online journal)

1. Introduction

Semiconductor quantum dots (QDs) have high potential in the fabrication of new quantum effect devices such as QD lasers and QD solar cells [1–8]. Semiconductor material has to be scaled down to the nanometer level comparable to the Bohr radius (Si Bohr radius: 4.9 nm) to generate the quantum effect. In this case, carrier wavefunctions are localized in nanomaterials and continuum bands are reduced to discrete quantum levels (the quantum size effect), which provides the opportunity to engineer the optical bandgap by adjusting the carrier confinement in spatial dimensions from size control [9–11]. A QD multi-layer is a promising absorber that generates photon-induced carriers, making it applicable

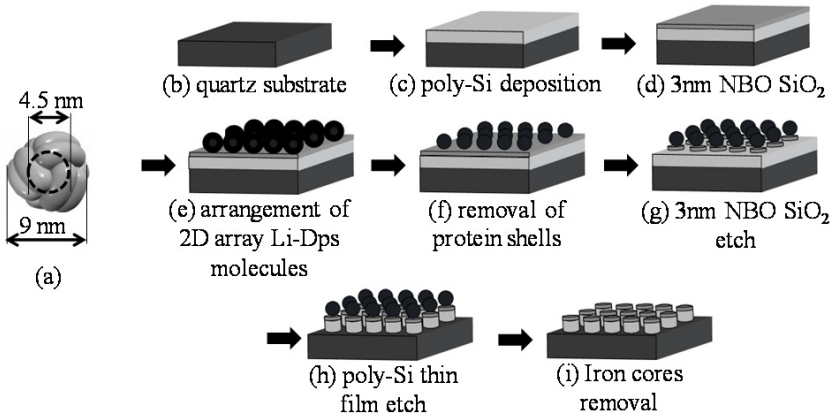

Figure 1. (a) Li-Dps with 4.5 nm diameter iron oxide core. (b)–(i) Fabrication flow of 2D array of Si-NDs by using NB etching with 2D array Li-Dps template.

to solar cells. All-Si tandem solar cells and intermediate band solar cells comprising QDs have attracted a great deal of attention for their potential to break through the Shockley–Queisser limit and their compatibility with current Si technology [12, 13]. Precisely controlling the size of QDs provides each cell with a different optical bandgap that can absorb various energy range photons of the solar spectrum. However, due to the finite device thickness, which is limited by the carrier transport process, high-density QDs are essential for improving optical absorption efficiency for fabricating tandem solar cells and intermediate band solar cells.

In the conventional technique, which is widely used to fabricate Si QDs, multiple layers of amorphous silicon-rich oxide (SiO_x, $x < 2$) and stoichiometric silicon dioxide (SiO_2) are alternately deposited using sputtering or plasma-enhanced chemical vapor deposition followed by annealing at a high temperature (usually 1100 °C) [14–16]. Silicon precipitates from the supersaturated solid solution and form nanocrystals. However, the results show poor uniformity of dot size and spacing, which indicates a limited control of quantum confinement. Furthermore, the QD density is not sufficiently high. It is still very difficult to control QDs precisely using this bottom-up process, which barely satisfies the strict requirements for fabricating realistic solar cells.

To overcome these problems, we have developed a top-down process utilizing a bio-template as a 7 nm diameter etching mask and damage-free neutral-beam (NB) etching for fabricating a sub-10 nm silicon-nanodisc (Si-ND) array structure as a QD. The structure shows distinct quantum effects, such as confined electron level dependence on the size effect, even at room temperature (RT) [17–20]. This structure has two geometrical parameters (thickness and diameter) that can be controlled independently. We previously fabricated a well-ordered arrangement of high-density 2D Si-ND by combining a bio-template etching mask of a 7 nm diameter etching mask ferritin core array with NF_3 gas/hydrogen radical treatment (NF_3 treatment) and Cl damage-free NB etching [21, 22]. The optical characteristics show that reducing only the Si-ND structure thickness (from 12 to 2 nm) enabled the optical bandgap energy (E_g) to be adjusted between 1.3 and 2.2 eV [22]. In this study, to fabricate an ND structure we have first used a new 2D array bio-template of *Listeria*-Dps (Li-Dps) as the etching mask like shows in figure 1(a). Li-Dps is a Dps protein that is synthesized from *Listeria* bacteria. It has a spherical protein shell with a cavity diameter of 4.5 nm and biomineralizes iron as an hydrate iron oxide core (diameter: 4.5 nm) in the cavity and stores it. By using iron oxide core as the 4.5 nm diameter etching mask, we would like to realize a much smaller diameter size of the Si-ND structure. Then we investigated the controllable range of E_g and optical absorption characteristic by changing the Si-ND diameter. To discuss and understand the mechanism, we also compared the experimental result with the simulation result.

2. Experimental details

The fabrication of a 2D Si-ND array structure using the new bio-template (Li-Dps) and damage-free NB etching is schematically shown in figures 1(b)–(k). The fabrication steps are as follows. First, 4 nm thick poly-Si and 3 nm thick silicon dioxide (SiO_2) layers were fabricated on a 10 × 10 mm^2 quartz substrate as shown in figures 1(b)–(i). The poly-Si layer was prepared using molecular beam epitaxy with a controlled deposition rate of 0.05 nm min^{-1} followed by annealing in argon atmosphere at 600 °C for 16 h. By *in situ* monitoring the poly-Si deposition thickness we could precisely control the thickness of the Si-ND. Then a 3 nm SiO_2 layer was fabricated using our developed neutral-beam oxidation process at a low temperature of 300 °C as a surface oxide (hereafter called 'NBO SiO_2') [23]. Second, a new bio-template of a 2D array of Li-Dps (a cage-shaped protein that has a 4.5 nm diameter iron oxide core in the cavity) molecules was formed through directed self-assembly on the NBO SiO_2 surface, as shown in figure 1(e). Two interactions should be considered during the formation of a high-density 2D array of Li-Dps molecules: between Li-Dps and the substrate. The latter is the main interaction. When the Li-Dps is dropped onto a highly hydrophilic NBO-SiO_2 surface, the Li-Dps solution spreads over the substrate. Li-Dps is negatively charged, which makes it dispersive in the solution. Since the NBO-SiO_2 surface is highly negatively charged, which makes it also dispersive in

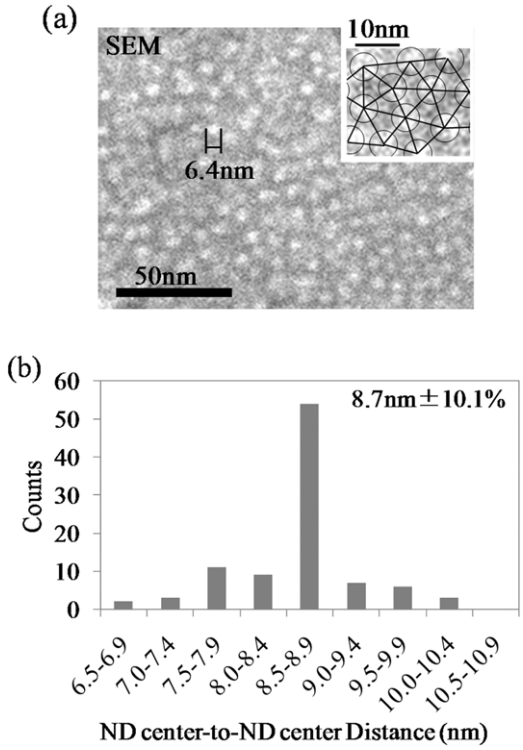

Figure 2. (a) SEM image of 2D Si-NDs array using Li-Dps. ($>1.4 \times 10^{12}$ cm^{-2}, diameter: 6.4 nm). (b) Distribution of ND-center-to-ND-center distances (8.7 nm ± 10.1%).

the solution, the electrostatic force suppresses the absorption of Li-Dps molecules onto the substrate. Transmission electron microscopy (TEM) results suggest that Li-Dps molecules have an attractive force between them when they are in the vicinity. Therefore, when the water meniscus pushes the Li-Dps down to the substrate during drying, the Li-Dps attains a sufficient degree of freedom of movement and easily reforms the arrangement to make a well-ordered, high-density and single-layer array. Next, Li-Dps protein shells were removed by heat treatment in oxygen atmosphere at 500 °C for 1 h to obtain a 2D array of iron oxide cores as the etching masks, as shown in figure 1(f). Etching was carried out by combination between isotropic etching of 3 nm NBO SiO_2 using NF_3 gas/hydrogen radical at 100 °C (hereafter called 'NF_3 treatment'), and anisotropic etching of poly-Si using Cl_2 NB, respectively, as shown in figures 1(g) and (h). Finally, the 2D iron oxide core array was removed using hydrochloric solution to obtain a 2D Si-ND array structure, as shown in figure 1(i). Because the native oxide grows between Si-NDs, we call this structure simply an 'Si-ND array structure with a SiO_2 matrix'. For comparison, we also prepared a 4 nm thick Si-ND array structure with a SiO_2 matrix by using ferritin (7 nm diameter iron oxide core). During the etching process by changing the NF_3 treatment time to 15 min and 40 min we could change the diameter due to the side etching of NBO-SiO_2 [24].

3. Results and discussion

After the etching process, the fabricated 2D Si-ND array structure using Li-Dps as the etching mask was observed using a scanning electron microscope (SEM, Hitachi 5200S). Figure 2(a) shows a top-view SEM image of the 2D Si-ND array structure fabricated using Li-Dps as the etching mask, which consisted of a closely packed array of 4.5 nm diameter iron oxide cores on the NBO SiO_2 surface. As the figure shows, this array structure had a high density (1.4×10^{12} cm^{-2}), uniform size (Si-ND diameter: 6.4 nm) and well-ordered arrangement (quasi-hexagonal ordered arrays). The density of a 2D Si-ND array structure fabricated for comparison using an etching mask of ferritin (7 nm diameter iron oxide core) was 7.0×10^{11} cm^{-2} (NF_3 treatment time: 40 min, Si-ND diameter: 10.5 nm). The density of the 2D Si-ND array structure fabricated using Li-Dps increased to two times that of the array fabricated using ferritin, while the diameter of the Si-ND shrunk to 61% of that obtained by using ferritin with 40 min NF_3 treatment. To confirm regularity in this array, we measured the center-to-center distance between adjacent Si-NDs, as shown in the SEM image in figure 2(a). Figure 2(b) shows that the absolute value of the center-to-center distance and its standard deviation were 8.7 nm and 10.1%, respectively. The results show that the 2D Si-ND array structure fabricated using a Li-Dps etching mask with a 4.5 nm diameter iron oxide core formed a 2D superlattice structure with a highly density and well-ordered arrangement, making it a suitable quantum dot structure.

The structure's optical absorption properties were studied by measuring the transmittance of samples. Optical absorption of the 2D Si-ND arrays was recorded using a JASCO ultraviolet–visible–near-infrared spectrometer. The transmittance absorption coefficient was calculated on the basis of the equation [25]

$$\ln(I_0/I) = \alpha d \tag{1}$$

where α is the absorption coefficient, d is the Si-ND thickness, I_0 is the intensities of incident light and I is the transmitted light, respectively. To determine the optical bandgap energy, we used the Tauc formula [26–28]

$$(\alpha h\nu)^n = A(h\nu - E_g) \tag{2}$$

where A is a constant, h is Planck's constant, ν is frequency, E_g is the optical bandgap energy and n is 1/2 in the case of indirect allowed electronic transitions. Figure 3(a) shows the Tauc plot ($(\alpha h\nu)^{1/2}$ versus photon energy ($h\nu$)) of the Si-ND array structures 6.4 nm (NF_3 treatment time: 15 min, Li-Dps: 4.5 nm diameter iron oxide core) and 10.5 nm (NF_3 treatment time: 40 min, ferritin: 7.0 nm diameter iron oxide core) in diameter combined with an SiO_2 matrix. These plots have a distinct linear region that indicates the onset of absorption. Therefore, extrapolating this linear region to the abscissa of photon energy gives the energy of E_g of the 2D array of Si-NDs. Figure 3(b) shows the fitting region of each ND thickness and its coefficient of determination (R^2). The fitting error for both lines is less than 0.16%, which means a very high accuracy. By shrinking the Si-ND diameter from 12.5 to 6.4 nm, the optical bandgap increased from 1.8 to 1.9 eV even at a disc thickness of 4 nm. On the basis of these results, we summarized that the relationship between the E_g and the Si-ND diameter, as shown in figure 3(c). In figure 3(c) we

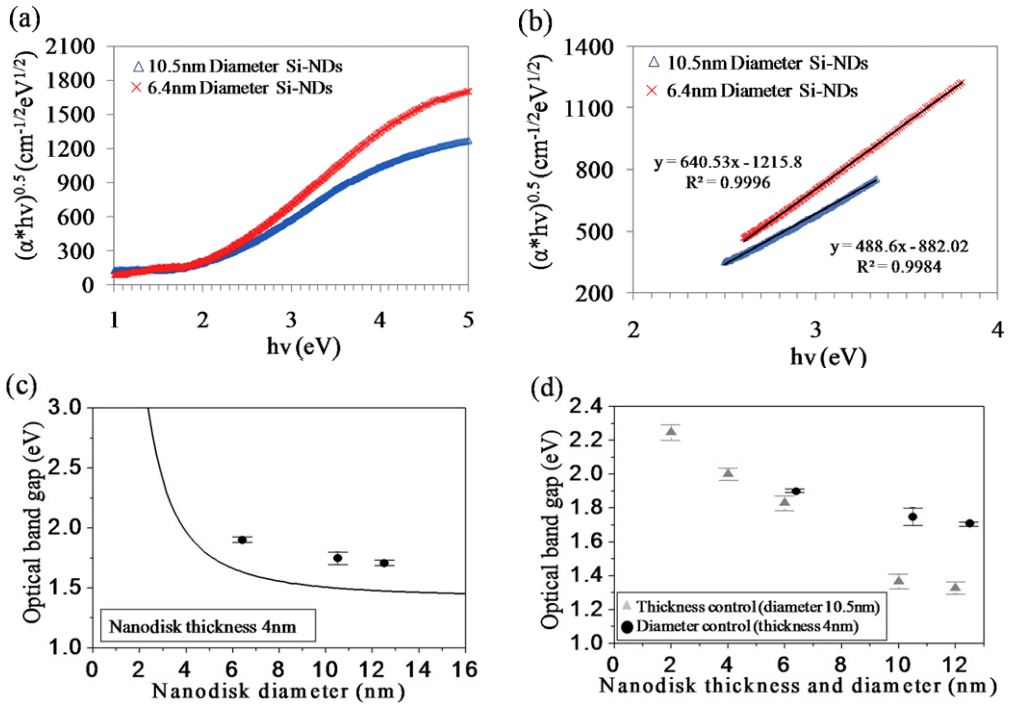

Figure 3. (a) Tauc plot of diameters 6.4 and 10.5 nm Si-NDs with SiO_2 matrix. (b) Linear trendline fitting area of Tauc plot diameters 6.4 and 10.5 nm Si-NDs with SiO_2 matrix. (c) E_g controlled by the function Si-ND diameter (ND thickness: 4 nm) and E_g calculation result (ND thickness: 4 nm). (d) Comparison of E_g by the function of Si-ND thickness control (ND diameter: 10.5 nm) and Si-ND diameter control (ND thickness 4 nm).

also put E_g of ND with 12.5 nm diameter (NF_3 treatment time: 15 min, ferritin: 7.0 nm diameter iron oxide core). These results clarified that quantum confinement in the Si-ND array structure occurred in diameter directions for the first time. The theoretical result is also inserted in figure 3(c). With the classic envelope-function theory, we solve the one-band Schrödinger equations to get the electronic structure of our Si-NDs:

$$-\nabla \cdot \left(\frac{h^2}{2m}\nabla\phi\right) + V\phi = E\phi \tag{3}$$

where h, mV, E, ϕ are Planck's constant, the effective mass, the position-dependent potential energy, quantum levels and the electron envelope function, respectively. Our calculations reveal that, due to the classic quantum localization effect, the ND bandgap gradually decreases with increasing diameters which matches with experimental data. It proved that controlling diameter is a feasible bandgap engineering method. A slight difference mainly comes from that the level gap between the heavy hole and electron underestimated the electronic bandgap; in contrast, due to the complex band edge effect, the optical bandgap energy deduced from absorption spectra was slightly larger than the electronic bandgap. The bandgap (E_g) is the uppermost property of semiconductors which is differed from metals and insulators, which determines their special electronic/optical properties and wide device applications. By combining our previous result [22] and the new experimental result of figure 3(c), we found that the E_g could be controlled by both Si-ND thickness and diameter, as shown in figure 3(d). The diameter from 6 to 10 nm allowed the E_g to be changed in the range of 0.2 eV, while controlling the thickness from 6 to 10 nm allowed the gap to change in the range of 0.5 eV. This result also suggests that stronger quantum confinement occurs in the thickness direction. These results made it clear that independently changing the geometric parameters of thickness and diameter in our proposed Si-ND array structure enables the optical bandgap to be precisely designed within a wide range. It is known that the conventional QD technique, i.e. a solution-precipitation method that is subject to chemical reaction and Stranski–Krastanov (SK) growth that is based on stress, cannot achieve independent two-dimensional quantum control with a high degree of precision.

As for an application in solar cells, the photon utilization efficiency depends on the optical absorption coefficients. Figure 4(a) shows the normalized optical absorption coefficient of Si-NDs. The result reveals that the 2D Si-ND array structure fabricated using Li-Dps (Si-ND diameter: 6.4 nm) had a higher absorption coefficient, more than two times the peak value, than that fabricated using ferritin (Si-ND diameter: 10.5 nm). The uniformity of the measured five points is shown in figure 4(b). For 6.4 nm diameter Si-ND absorption coefficient the uniformity at $E_g = 1.9$ eV is 1.4×10^4 cm^{-1} $\pm$ 12%.

To enable better understanding of the photon utilization efficiency, we defined an integrated area of absorption coefficient from the E_g to 5.0 eV. Figure 5(a) shows the normalized thickness control result, where the integrated area of absorption coefficient decreased from 1.1 to 0.7 arb. unit when the thickness was decreased from 12 to 2 nm. With respect to the diameter control, the integrated area absorption coefficient increased about 2.2 times (from 1.0 to 2.2 arb. unit)

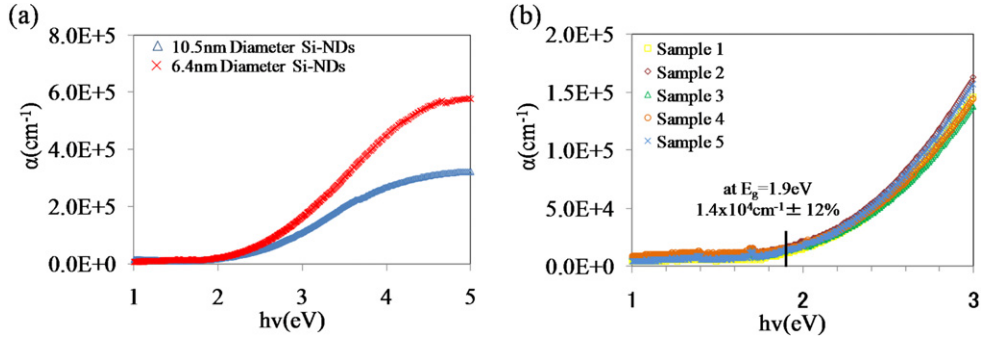

Figure 4. (a) Absorption coefficient of 6.4 and 10.5 nm diameter Si-NDs with SiO_2 matrix. (b) The absorption coefficient's uniformity of 6.4 nm diameter Si-NDs with SiO_2 matrix (absorption coefficient at $E_g = 1.9$ eV is 1.4×10^4 cm^{-1} $\pm$ 12%).

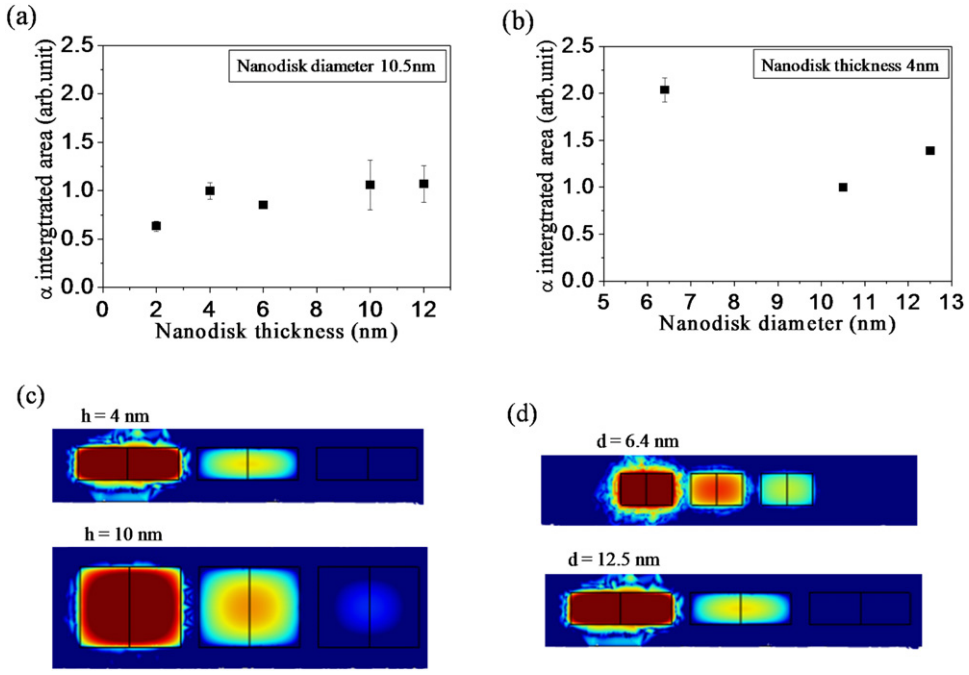

Figure 5. (a) Integrated absorption coefficient by the function of Si-ND thickness with SiO_2 matrix (ND diameter: 10.5 nm). (b) Integrated absorption coefficient by the function of Si-ND diameter with SiO_2 matrix (ND thickness 4 nm). (c) Simulation result of wavefunction coupling of thickness control in ND array structure (ND thickness, $h = 4$ and 10 nm). (d) Simulation result of wavefunction coupling of diameter control in ND array structure (ND diameter, $d = 6.4$ and 12.5 nm).

when the diameter was decreased from 12.5 to 6.4 nm, as shown in figure 5(b). These results indicated that, when using ferritin as the etching mask material, the decreased thickness caused decreased optical absorption. However, using Li-Dps to fabricate even very thin 2D Si-ND arrays allows high optical absorption while keeping a higher optical bandgap.

This interesting phenomenon is perhaps attributed to the lateral coupling of NDs. Strongly coupled wavefunctions do not only discretize the initial quantum level but also relax selection rules to induce additional transitions, which commonly means an increased state density and leads to an enhanced total absorption. Within the envelope-function theory (equation (3)), we calculated electron spatial possibilities (square wavefunction) in three lateral coupled NDs according to our sample structures. Several results are shown as the logarithmic axis in figures 5(c) and (d). In figure 5(c), we could not observe any significant changes in wavefunction coupling in the case of changing the ND thickness. The vertical potential width is mainly to control the vertical wavefunction distribution. Many researchers have decoupled a 3D Schrödinger equation to three 1D Schrödinger equations. Thus, changing thickness cannot markedly change the lateral coupling strength and finally results in a very small change in the absorption coefficient. In contrast, in the case of decreasing the diameter, wavefunction coupling is effectively enhanced, as shown in figure 5(d). A possible reason is that, by decreasing diameters, the center-to-center distance between NDs is decreased so that wavefunctions more easily spread to the neighboring NDs and are coupled with each other. With the Kronig–Penny model, Green *et al* also proved that decreasing the Si cubic size will increase the miniband width, which also means an enhanced wavefunction coupling [29]. Just like our previous analysis, this enhanced wavefunction coupling will enhance the total absorption.

4. Conclusion

We successfully fabricated a superlattice structure with small Si-NDs of 6.4 nm diameter and high Si-ND density of more than 1.4×10^{12} cm^{-2} by using our new process involving a bio-template 4.5 nm etching mask of (Li-Dps iron oxide core) and NB etching. The optical absorption coefficient was extremely high due to a small high-density Si-ND array structure and a controllable E_g with a wide range was achieved by controlling the Si-ND diameter and thickness. This new process is suitable for development of realistic all-Si tandem solar cells and Si intermediate-band solar cells.

References

[1] Zhuang L, Guo L and Chou S Y 1998 *Appl. Phys. Lett.* **72** 1205
[2] Sellin R L, Ribbat Ch, Grundmann M, Ledentsov N N and Bimberg D 2001 *Appl. Phys. Lett.* **78** 1207
[3] Schneider C, Strauß M, Sünner T, Huggenberger A, Wiener D, Reitzenstein S, Kamp M, Höfling S and Forchel A 2008 *Appl. Phys. Lett.* **92** 183101
[4] Ishikuro H and Hiramoto T 1997 *Appl. Phys. Lett.* **71** 3691
[5] Wood V, Panzer M J, Caruge J-M, Halpert J E, Bawendi M G and Bulovic V 2010 *Nano Lett.* **10** 24
[6] Chakrabarti S, Holub M A, Bhattacharya P, Mishima T D, Santos M B, Johnson M B and Blom D A 2005 *Nano Lett.* **5** 209
[7] Luque A and Marti A 2011 *Nature Photon.* **5** 137
[8] Luque A and Marti A 2009 *Adv. Mater.* **21** 160
[9] Yu H, Li J, Loomis R A, Gibbons P C, Wang L W and Buhro W E 2003 *J. Am. Chem. Soc.* **125** 16168
[10] Kongkanand A, Tvrdy K, Takechi K, Kuno M and Kamat P V 2008 *J. Am. Chem. Soc.* **130** 4007
[11] Pejova B and Grozdanov I 2005 *Mater. Chem. Phys.* **90** 35
[12] Conibeer G *et al* 2006 *Thin Solid Films* **511/512** 654
[13] Shockley W and Queisser H J 1961 *J. Appl. Phys.* **32** 510
[14] Hao X J, Podhorodecki A P, Shen Y S, Zatryb G, Misiewicz J and Green M A 2009 *Nanotechnology* **20** 485703
[15] Kurokawa Y, Tomita S, Miyajima S, Yamada A and Konagai M 2007 *Japan. J. Appl. Phys.* **46** L833
[16] Wen X, Dao L V and Hannaford P 2007 *J. Phys. D: Appl. Phys.* **40** 3573
[17] Samukawa S, Sakamoto K and Ichiki K 2002 *J. Vac. Sci. Technol.* A **20** 1566
[18] Samukawa S, Sakamoto K and Ichiki K 2001 *Japan. J. Appl. Phys.* **40** L997
[19] Matsui T, Matsukawa N, Iwahori K, Sano K, Shiba K and Yamashita I 2007 *Langmuir* **23** 1615
[20] Kubota T, Baba T, Kawashima H, Uraoka Y, Fuyuki T, Yamashita I and Samukawa S 2005 *J. Vac. Sci. Technol.* B **23** 534
[21] Huang C H, Igarashi M, Horita S, Takeguchi M, Uraoka Y, Fuyuki T, Yamashita I and Samukawa S 2010 *Japan. J. Appl. Phys.* **49** 04DL16
[22] Huang C H, Wang X Y, Igarashi M, Murayama A, Okada Y, Yamashita I and Samukawa S 2011 *Nanotechnology* **22** 105301
[23] Yonemoto M, Ikoma T, Sano K, Endo K, Matsukawa T, Masahara M and Samukawa S 2009 *Japan. J. Appl. Phys.* **48** 04C007
[24] Samukawa S, Kubota T, Huang C H, Hashimoto T, Igarashi M, Nishioka K, Takeguchi M, Uraoka Y, Fuyuki T and Yamashita I 2008 *Appl. Phys. Express* **1** 074002
[25] Pejova B and Grozdanov I 2005 *Mater. Chem. Phys.* **90** 35
[26] Tauc J, Menth A and Wood D L 1970 *Phys. Rev. Lett.* **25** 749
[27] He R and Tsuzuki T 2010 *J. Am. Ceram. Soc.* **93** 2281
[28] Singh S C, Mishra S K, Srivastava R K and Gopal R 2010 *J. Phys. Chem.* C **114** 17374
[29] Jiang C W and Green M A 2006 *J. Appl. Phys.* **99** 114902